A Novel Wireless Leaf Area Index Sensor Based on a Combined U-Net Deep Learning Model

Hancong Wang, Yin Wu, Qiang Ni, *Senior Member*, *IEEE*, and Wenbo Liu

***Abstract*—Leaf area index (LAI) is an important parameter for forestry vegetation canopy structure investigation and ecological environment model study. Traditional ground direct measuring method is too time and labor consuming, while the remote sensing technique lacks of adequate validation and comparative analysis. Here, a novel wireless LAI sensor based on a lightweight deep learning model (LAINET) has been designed with a Raspberry Pi microcomputer and a LoRa transceiver. The mainly metering pattern of sensor system is the digital hemispherical photography (DHP) methodology based on Beer-Lambert law: firstly, the crown canopy's image is captured and segmented by LAINET, then the vegetation gap fraction can be extracted to calculate the LAI value. Our proposed LAINET consists of a lightweight convolutional neural network (CNN) and a generative adversarial network (GAN). The average accuracy of semantic segmentation (i.e. CNN part) could reach 0.978, and the combination of GAN for image super-resolution reconstruction can improve the accuracy of gap fraction measurement more by 5.5%. In addition, LAINET effectively solves the problem of low segmentation accuracy brought by environmental effects, the separation accuracy in direct sunlight or clear weather has been improved significantly. So the ultimate LAI value can be calculated precisely and stably. Experiment results show that the proposed sensor obtains a fine measuring error of less than 4% when comparing with the commercial plant canopy analyzer HM-G20. Combined with Uninterruptible Power Supply module of 5200 mAh, the sensor can work effectively for about 8 months, principally meeting the deployment and measurement criteria of forestry LAI. Therefore, the wireless sensor presented in this paper has a great application prospect.**

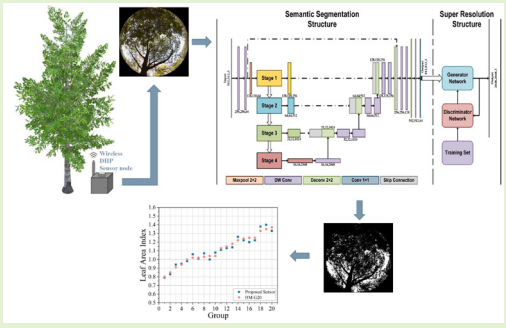

***Index Terms*—Leaf area index; Canopy fisheye image; Deep learning; Wireless sensor; Raspberry Pi.**

I. Introduction

Climate change has garnered considerable attention in recent decades. As an essential component of the global ecosystem, forests serve multiple functions, including air purification, climate regulation, and water conservation, etc. [1]. The leaf area index (LAI) is an important index used in the parameterization of forest vegetation structure and a key characteristic variable of the ecosystem function model [2]-[3]. Hence, accurate measurement of LAI can play a vital role in assessing the field water content, oxygen content, carbon storage and exchange of nutrients in the forest environment, which is of great significance for the efficient management and accurate monitoring of forest resources [4]-[5].

The main methods of LAI determination can be divided into two categories: direct and indirect [6]. Direct measurement is somewhat destructive and requires the collection of vegetative leaves with manual calculation. Since the direct measurement usually has a large workload, it is often used as the standard verification [7]. Among indirect methods, optical instruments are often used to measure certain intermediate parameters, from which, the LAI can be calculated by using the inversion formulas [8]. Current studies focus on using remote sensing technique or DHP to capture plant canopy images, thus the LAI can be deduced from plant canopy gap fraction, which is extracted by using image segmentation methods. The frequently used LAI-2200C plant canopy analyzer (LI-COR Inc., USA) adopts a fisheye lens to refract light within the hemispherical field of view to the photoelectric sensor, which is composed of five concentric circles [9]. But it is costly and inconvenient to carry. Jorge Mendes et al. designed a low-cost smartphone application to estimate the LAI that uses an ambient light sensor inside the smartphone [10]. Qu et al. designed and verified the effective-ness of LAISmart by measuring the LAI of four vegetation types: evergreen coniferous forest (ECF), deciduous broadleaf forest (DBF), deciduous coniferous forest (DNF), and broadleaf crops [11]. Brown et al. described the condition of ground vegetation using a low-cost UAV-based DHP system

This work was supported in part by the National Science Foundation of China (NSFC) under Grant No.32171788, No.31700478; Jiangsu Provincial Government Scholarship for Overseas Studies under Grant JS-2018-043, Innovation and Entrepreneurship Training Program for College Students in Jiangsu Province under Grant 202110298089Y (Design and Analysis of a Wireless Leaf Area Index Sensor).

Hancong Wang, Yin Wu are with the College of Information Science and Technology, Nanjing Forestry University, No.159, LongPan Road, Nanjing, 210037, P.R China (e-mail: hancong@njfu.edu.cn, wuyin@njfu.edu.cn).

Qiang Ni is with the InfoLab21, School of Computing and Communications, Lancaster University, Lancaster, LA1 4WA, UK (e-mail: q.ni@lancaster.ac.uk).

Wenbo Liu is with the College of Automation, Nanjing University of Aeronautics and Astronautics, No.29, JiangJun Avenue, Nanjing, 211106, P.R China (e-mail: wenboliu@nuaa.edu.cn).

[12]. However, all these methods require intense manual operation, which inhibits their application in the practical long-term forest monitoring scenario. With the development of low power wide area network technology [13], the remote automatic monitoring of forest LAI has become a research hotspot recently. Li et al. developed a LAI sensor that can continuously monitoring crop growth at multiple sampling points [14]. Moreover, 4G/Wi-Fi has also been adopted to remotely collect crop images in real time, then, after automatic image processing, LAI is calculated based on the improved Lang and Xiang LAI algorithm. Bauer et al. modified the commercial off-the-shelf photo synthetically active radiation (PAR) sensor that features feasibility, robustness, and low-cost, which has considerably improved the performance for non-destructive in situ LAI measurements [15]. Additionally, Kim et al. developed a smart surface sensing system which could automatically acquires, transmits and processes PAR and LAI data streams [16]. Fig. 1 just illustrates an application diagram using wireless sensors to monitor forest canopy parameters.

As the rapid progresses of micro-computer system and artificial intelligence algorithm in these years, convolutional neural networks (CNNs) demonstrate its advantages in image processing procedure, especially for semantic segmentation. Hence, it is also very suitable for the high-precision vegetation canopy image recognition. Li et al. proposed a low-cost LAI estimation method for early-stage winter wheat based on RGB images and deep learning [17]. This method meets the requirement of early LAI estimation, thus serves as a reference for growth status monitoring and agronomic management of winter wheat. Shu et al. achieved the LAI measurement of cucumber through an improved fully convolutional network (FCN) [18]. Ma et al. improved the segmentation performance of mapping learning model (Pix2pix), which showed good accuracy in LAI measurements [19].

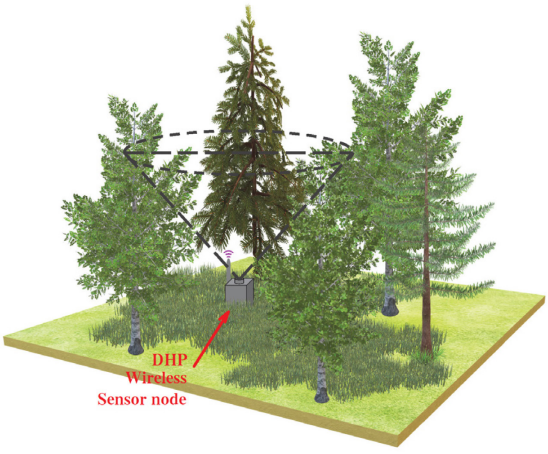

Fig. 1. Forest canopy parameter monitoring scenario using a wireless DHP sensor.

Nonetheless, current research still faces some difficulties. Primarily, traditional threshold segmentation method is unable to accurately obtain the optimal dividing value. The blue channels in the RGB images of sky and leaves are both the dominant parts, hence it is difficult to accurately distinguish the two items in a sunny environment. Even under cloudy days, it is also quite hard to separate the leaves from the background exactly. Fig. 2 shows the comparison results of HSV-based segmentation [20] and Otsu [21] method: Fig. 2(a) is the original image taken by the fisheye lens. The color of sky in the lower left is white due to the lighting conditions, while the color of sky in the upper right is blue. In Fig. 2(b), the brightness of these two sky regions are also different. Fig. 2(c) is the segmentation result of HSV-based method and Fig. 2(d) shows the Otsu's. Clearly, HSV gains good performance in the segmentation of fine details, but not very convincing for the boundaries between sky and leaves: For instance, the sky at the lower left corner has been erroneously divided into leaves. On the other hand, Otsu could not process effectively in the trivial gaps, the middle and lower parts of the image have been miscalculated and displayed too densely.

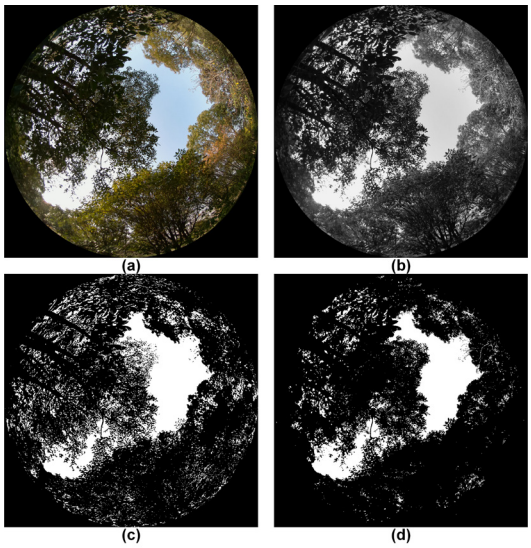

Fig. 2. (a) Original RGB image taken with 180° fisheye lens, (b) the fisheye image processed by grayscale, (c) the fisheye image processed by HSV threshold segmentation, (d) the fisheye image processed by Otsu threshold segmentation.

Besides, ordinary CNNs are not compatible for deployment on edge computing platforms, such as Raspberry Pi [22], due to the large number of model parameters and computing budget. While the existing lightweight neural network architectures always present low accuracy for binary semantic segmentation tasks [23] and do not meet the requirements for forest crown segmentation. Furthermore, CNNs have certain demands on the input size of treated images: those with a high resolution will increase the computation workload steeply and reduce the network prediction speed, whereas low-resolution images will lose a reasonable quantity of detailed information on forest canopy, as well as lowing the measurement accuracy.

Ultimately, the traditional hand-held LAI analyzer is bulky and inconvenient to carry out in the field. Although some former studies have successfully measured the LAI with portable devices, such as mobile phones, the measurements were completed manual operation, which is time-consuming and labor-intensive. Therefore, we propose a novel LAINET architecture that combines the advantages of traditional and lightweight CNN, subsequently followed by a super resolution GAN (SRGAN) [24] to super recover the detail information of its output image. The proposed model could effectively reduce the environmental effects of hemispheric photography through data augmentation and training procedures. It can be deployed on a Raspberry Pi connecting with one fisheye camera, one

LoRa communication module, and a battery power module, just a formal wireless measuring node that can realize remote, real time, and automatic LAI monitoring.

The manuscript is described as follows: Section II explains the LAI measurement principle, including the theoretical model based on the Beer-Lambert law, our investigation site and the hardware-software implementation of proposed node. Section III presents the lightweight LAINET algorithm for extracting forest gap fraction. Section IV details the performance of LAINET on plant canopy image segmentation, also a result comparison with the hand-held LAI analyzer has been included. At last, Section V summarizes our findings and draws the outlook.

II. LAI Measurement Method

A. Theoretical Background

In the natural environment, plant leaves are randomly distributed, the surface area of a single leaf is much smaller than the total area of the vegetation canopy, and the angle of inclination of each leaf is hybrid. Thus, the vegetation canopy can be approximated as a light-transmitting solute. According to the Beer-Lambert law, the LAI can be derived from the perspective of solar radiation intensity attenuation. The parametric model is shown in Fig. 3.

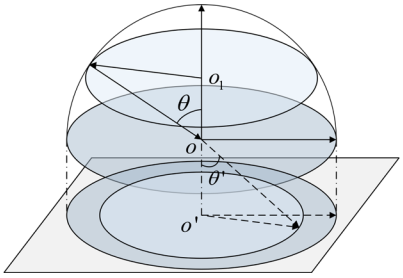

Fig. 3. Structural parameter model based on hemispherical photography.

The semicircular sphere in the upper part of the figure is the fisheye lens model, and the lower part is the imaging model. o is the center of sphere of fisheye lens, and θ is the zenith angle. o_1 is the center of circle plane when zenith angle is θ. Ray of light is refracted and taken into the lens at angle θ, afterwards it is emitted at an angle of θ' and imaged into the photograph. o' is the center of photographic image.

Assume that the resulting photo has only the vegetation and sky, $T(\theta)$ is the gap fraction of vegetation when the zenith angle is θ, $N_v(\theta)$ is the total number of pixels of vegetation in the area, and $N_s(\theta)$ is the total number of pixels of sky, then:

$$T(\theta) = \frac{N_s(\theta)}{N_s(\theta) + N_v(\theta)} \tag{1}$$

$G(\theta)$ is the value of vegetation projection function when the zenith angle is θ:

$$LAI = -\frac{lnT(\theta) \cdot cos\theta}{G(\theta)} \tag{2}$$

Due to the randomly distribution of most tree leaves, the leaf inclination angle is not a fixed value. However, when the zenith angle is around 57.5°, the projection function value at any leaf inclination angle is about 0.5. Therefore, it can be regarded that the projection function value is independent of the leaf inclination angle (i.e., θ = 57.5 and $G(\theta)$ = 0.5) [25]. To calculate the LAI using intelligent machine vision, the ring at ~57.5° can just be used for analysis, then $N_v(\theta)$ and $N_s(\theta)$ are the number of pixels of vegetation and sky within the circle, respectively. So the size of the ring area would greatly affect the calculation results. If the ring angle is too large, the feature at 57.5° will be weakened and the projection function will be shifted. If the ring angle is too small, effective plant canopy information from the ring may not be able to be well extracted. Based on empirical experience, a ring of 55–60° is suitable for the extraction of plant canopy gap fraction. Hence,

$$LAI = -\frac{lnT(57.5°) \cdot cos57.5°}{0.5} \approx -lnT(57.5°) \tag{3}$$

where $T(57.5°)$ is the ratio of the number of background pixels to the total number of pixels in the 55-60° ring. Since only the characteristics at 57.5° were used in the analysis, it is referred as the single angle method. This method is highly efficient and cost effective to obtain the LAI reliably. Thus, it has been appropriately used in various studies [26].

B. Investigation Area

The forest canopy images in this study were collected in the Zhongshan Botanical Garden, Nanjing, China, from October 2021 to May 2022 (31°14′-32°37′N, 118°22′-119°14′E). The area of the garden is about 186 hectare, and the climate is mild. It belongs to the north subtropical monsoon climate zone, with an average annual temperature of 14.7℃.The rich abundance of plant species ensures the diversity of living tree samples in this study. Images were collected using the proposed wireless DHP sensor and a HM-G20 commercial plant canopy analyzer [27] was adopted for the verification. Fig. 4 shows the geographical environment of our experiment site.

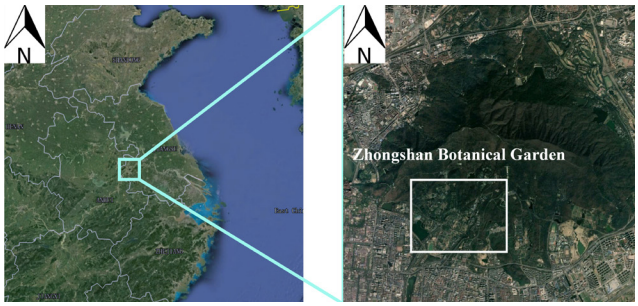

Fig. 4. Location and geographical environment of our experiment area.

C. Structure and Workflow of the Proposed Wireless Sensor

The Raspberry Pi is a microcomputer based on ARM® architecture. It has sufficient number of extension I/O ports, and is suitable for certain tasks, such as sensor node design and edge computing. It is equipped with the Raspberry Pi OS based on the Linux system, which is convenient for debugging and developing software programs. In this study, a Raspberry Pi 4B is used as the central computing unit of the wireless sensor. The related parameters are shown in Table I.

Three function modules have been connected with the Raspberry Pi through the extension I/O ports. The forest canopy image is captured using a fisheye lens with field view angle of 200°. The image CMOS sensor is OV5647 with 1/4 inch size and 0.87 mm focal length [28]. Its maximum image resolution is 2592 × 1944. A LoRa® module is adopted for the information transmission by reason of its properties in low power consumption and long communication distance. In terms of power supply, a 5200 mAh UPS battery module is employed. The whole physical prototype of the sensor is shown in Fig. 5.

Fig. 6 shows the workflow of proposed wireless DHP sensor. Firstly, the RGB images of forest canopy are collected by the fisheye lens, which should be preprocessed to a predefined dimension and classified to a training dataset. Note that prior to LAINET training, data augmentation must also be carried out to increase the number of samples and enhance the data diversity which aims to strengthen the system's robustness to negative environmental factors such as direct sunlight. Subsequently, to perform LAI estimation, the pretreated images are imported into LAINET for semantic segmentation and the diagnose system would calculate the gap fraction based on the partition results. Then LAI can be calculated effectively by the single angle method and the optimal detecting model would be stored. Finally, DHP sensor uploads the real-time LAI testing result to the network server remotely.

Fig. 5. Prototype of the proposed wireless DHP sensor.

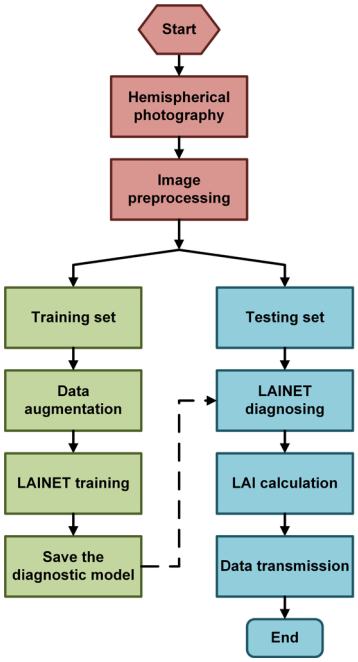

Fig. 6. Workflow of the proposed wireless DHP sensor.

III. The Proposed LAINET

A. Data Pre-processing

TABLE I
SOME PARAMETERS OF RASPBERRY PI 4B

Content	Raspberry Pi 4B
SOC	BCM2711B0
CPU	ARM Cortex-A72 4-Core 1.5GHz
GPU	Broadcom VideoCore IV@500MHz
RAM	8G LPDDR4
Power	5V 3A
Size	85 x 56 x 17 mm

The process of data pre-processing is divided into two aspects: image pre-processing and data augmentation, as shown in Fig. 7. The purpose of pre-processing is to modify the images to fit the input size of LAINET; Data augmentation, on the other hand, is to solve the problem of small sample data set amount.

1) *Image Pre-processing*

The resolution of the picture taken by Raspberry Pi lens used in this study is 2592 × 1944, while the actual imaging part of the fisheye lens is theoretically a circular area, so it is necessary to pre-process the image first, remove the excess black edges on the left and right sides, and cut out the actual visible circular area. Another problem is that due to the effect of manufacturing process, the imaging center of fisheye lens is not necessarily the center of DHP image, so the pixel marked (1296, 972) cannot be directly selected as the center of the circle. According to practical experience, we select the image with a field angle of 180° and compresses its resolution to 512 × 512, so as to input it into the neural network. As shown in green part of Fig. 7, the specific methods are: (1) traversing the pixel from left to right according to column; (2) finding the location of the first color pixel; (3) finding the location of the last color pixels; (4) the symmetry center of these two pixels is just the fisheye image center, while the radius could be calculated based on the position of this center and the two extreme pixels. In fact when in field testing, due to the light diffraction, there is a gray-black area around the fisheye image, which can have a certain effect on the traversal of pixels. But since the number of pixels on the long side of the original image (2592) is much larger than the compressed image (512), this error is basically negligible. (5) So after obtaining the center and radius, a hemispherical image with a field view of 180° can be captured. This image is a square and the side length is the diameter of the fisheye image. Lastly, the resolution of the image should be compressed to 512 × 512.

2) *Data Augmentation*

Manually labeling forest canopy images is a tedious task and it is nearly impossible to obtain substantial samples for the neural network training within a short period of time. Therefore, it is necessary to augment the data to quickly obtain a large number of training samples. Traditional data augmentation methods include rotation, flipping, translation, and cropping. In this study, based on the actual imaging environment conditions,

random noise and color dithering are also selected.

As the camera lens is directly exposed to the air, it may be contaminated by dust particles in the wind and water stains left by rainfall. In addition, if the sensor circuit overheats, it will generate a certain amount of noise. These factors have a certain influence on the imaging performance of the fisheye lens. So noise must be introduced in the image pre-processing to achieve near perfect data augmentation, and the neural network can be trained to distinguish the noise from the original image. Considering all these drawback conditions, Salt-Pepper noise and Gaussian noise are adopted here. Salt-Pepper noise is used to simulate the pollutant at lens surface and Gaussian noise is used to imitate the noise generated during signal transmission procedure.

Previous studies have mentioned that when the LAI value is measured under direct sunlight, it differs considerably from the actual number. Therefore, it is necessary to minimize the effects of illumination on the measurement as sunlight often leads to image color variations. Here the color dithering mechanism has been chosen to reduce the influence of lighting conditions on the segmentation results. It is mainly achieved by changing the image contrast, brightness, and saturation during this training section.

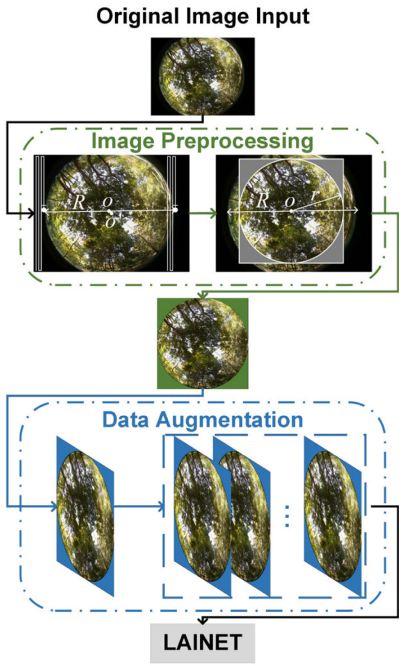

Fig. 7. Data pre-processing process.

B. The Proposed LAINET

In the proposed study, a deep learning model LAINET based on CNN and GAN is presented. The CNN part adopts a lightweight semantic segmentation structure based on U-Net [29], ResNet50 [30] and MobileNetV1 [31] models, whose role is to segment the forest canopy fisheye images with a resolution of 512 × 512.The GAN part adopts a SRGAN model, which aims to super-resolution the CNN's output to 2048 × 2048, thus improving the accuracy of gap fraction calculation. The overall architecture of LAINET is shown in Fig. 8.

1) *CNN Architecture*

The LAINET employs the U-shaped symmetric structure of U-Net. The U-Net model (Fig. 9(a)) can effectively solves the problem of binary semantic segmentation while extract deep and shallow information. Moreover, U-Net is suitable for small sample data training, which perfectly meets the segmentation requirement of forest canopy image sets. Here the dimension standard of input and output images of U-Net have been adjusted, as the original parameters are effective for medical image segmentation, but not for the forest canopy images.

The contracting feature extraction network of U-Net is composed of five layers. In each layer, two convolutions are used to increase the number of feature layers. The maximum pooling operation is performed between one layer and the next to reduce the image size. The network structure is similar to VGG16 [32] without the fully connected layer. The advantage of this structure is that the network is simple and only uses two operations, 3 × 3 convolution and 2 × 2 maximum pooling. Its

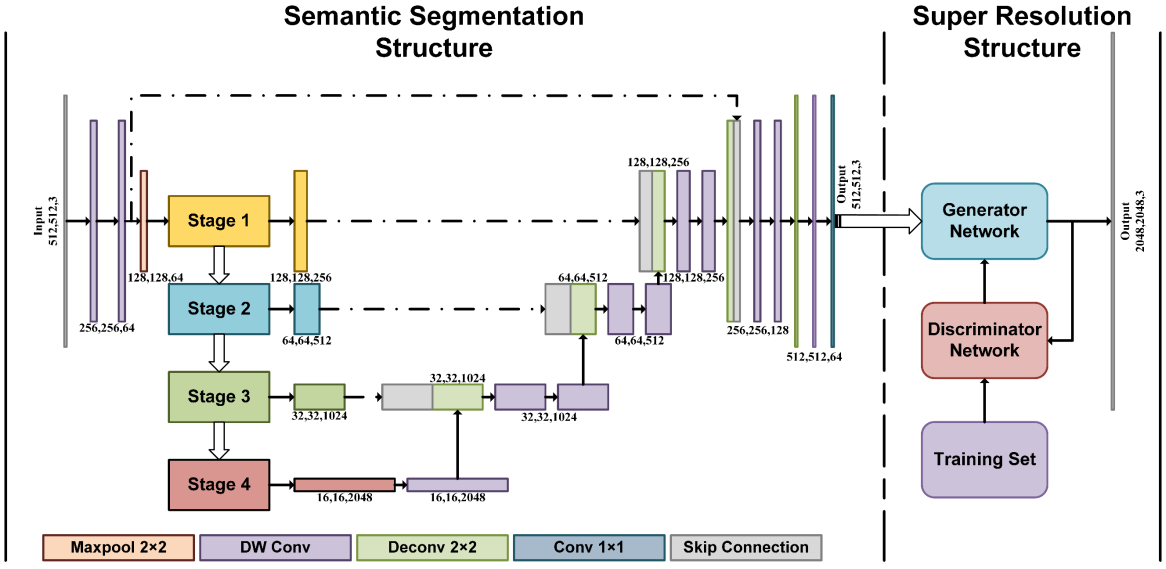

Fig. 8. Frame structure of the proposed lightweight deep learning network LAINET.

disadvantage is that the depth of network is not deep enough to extract the insightful feature information. By simply increasing the number of convolutional layers to improve the depth of network, it is unable to achieve the desired result. Because as the network depth increases, the accuracy of the training set tends to decrease while the error rate increases, which is called the "degeneration" problem. To address this issue, ResNet50 and so forth models have been designed. Hence, in order to further extract deep information of the forest canopy image, here the original VGG16 structure is replaced by a structure similar to ResNet50. Meanwhile, in order to meet the requirements of feature fusion, this paper also adjusts the input parameters of corresponding layers in the extended feature extraction network, so that feature images complete in each step of ResNet50 training can be fused with corresponding deconvolution layers through skip connection. The ResNet50 corresponding structure used in LAINET is shown in Fig. 9(b).

MobileNetV1 displayed the core of depthwise separable convolution (Fig. 9(c)). Through this architecture, the amount of computation can be significantly reduced. In our research, depthwise separable convolution is also introduced to replace the general 3 × 3 convolution in the expanding feature extraction part to reduce the number of network parameters of LAINET, thereby reducing the memory usage and requirements on computing power.

Thus, we present the LAINET, which jointly combines the advantages of U-Net, ResNet50, MobileNetV1, and has an optimized structure for the LAI measurement. The input image resolution of LAINET is 512 × 512; the size is first compressed to 8 × 8 through the feature extraction network and the number of feature layers increased from 3 to 2048, which is much higher than the 1024 layers in U-Net. Then, the original resolution was restored through the feature extraction network and semantic segmentation of each pixel was achieved through a prediction network composed of a 1 × 1 convolution so that the output image has the same resolution as the original image.

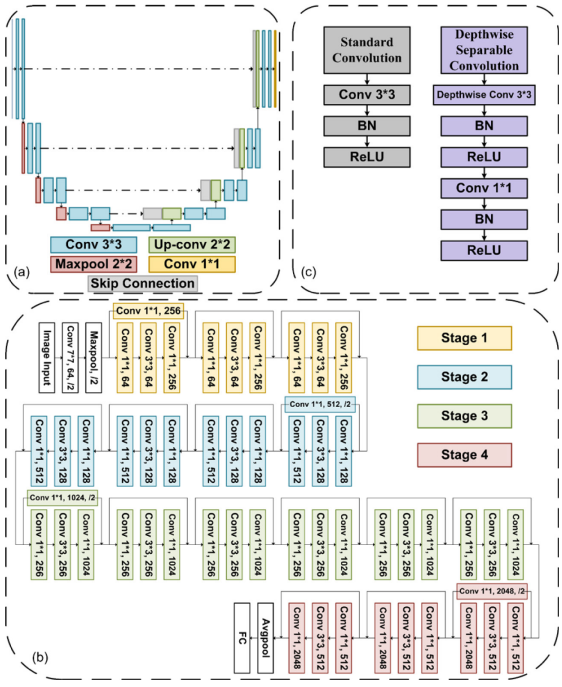

Fig. 9. The structure of (a) U-Net, (b) ResNet50 and (c) Depthwise separable convolution of MobileNetV1 used by LAINET.

2) *GAN Architecture*

Raspberry Pi has limited computing power for the semantic segmentation of high-resolution images, so we must compress the input image resolution to 512 × 512 for deep learning. However, on one hand, low resolution images cannot reflect the deep feature of forest canopy, and the segmentation result always has a strong jaggedness, which is significantly different from the actual perception; on the other hand, the weight of individual pixels in low resolution image is larger, and incorrect segmentation will have a greater impact on the calculation of gap fraction, so the image should be restored to high resolution to enhance the identification accuracy. In recent years, GAN has been widely used in the image super-resolution task [33], and the advanced SRGAN model is recommended in this study, as shown in Fig. 10.

GAN consists of generator network and discriminator network. The structure of generator network is shown in Fig. 10(a). Firstly, the input low resolution image goes through a convolution and a ReLu activation function. Then it enters a residual network structure which consists of several residual blocks, each residual block contains two convolutions, two batch normalization and one ReLu activation function inside. Finally, two up-sampling procedures are performed to increase the resolution of the original one. The discriminator network, on the other side, consists of constantly repeated convolution, Leaky ReLu activation function, and batch normalization operation, as shown in Fig. 10(b). In order to reduce the number of network model parameters, we replace some of the ordinary convolution by depthwise separable convolution.

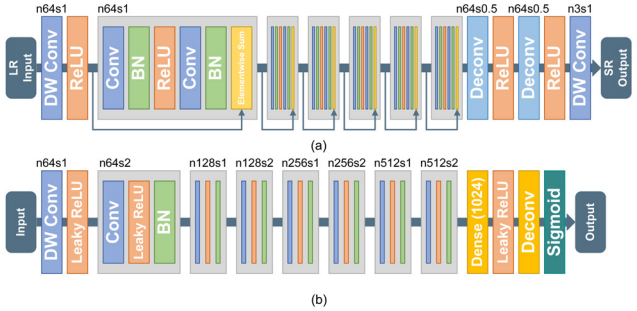

Fig. 10. Frame structure of the proposed lightweight SRGAN.

During the GAN training stage, low resolution images are inputted into the generator network, and corresponding high resolution images are inputted into discriminator network. Through a series of established operations, the generator would generate high-resolution images and ask the discriminator to determine whether they are true or not. After certain groups of training, the generator could generates images that are realistic enough for which the discriminator are unable to distinguish. Hence the generator training process can be completed. The so trained generator model will be saved and a super-resolution image can be obtained by inputting the image into the generator networks during actual deployment.

C. Evaluation Metrics

According to the confusion matrix, there are two types of true values: Positive and Negative; two types of predicted values:

True and False. Therefore, there are four possible outcomes: (1) True-Positive (TP), (2) True-Negative (TN), (3) False-Positive (FP), and (4) False-Negative (FN). The following formulas are used to calculate the ACC (accuracy), Recall, Precision and F1_score:

$$ACC = \frac{TP + TN}{TP + TN + FP + FN} \tag{4}$$

$$Recall = \frac{TP}{TP + FN} \tag{5}$$

$$Precision = \frac{TP}{TP + FP} \tag{6}$$

$$F1\_score = \frac{2 \times Precision \times Recall}{Precision + Recall} \tag{7}$$

ACC is the most popular indicator. Generally, the higher the ACC, the better the network performance. In this study, ACC represented the accuracy of semantic segmentation of plant canopy gap fraction. However, since calculation of the LAI does not require gap location information, ACC does not directly indicate the LAI calculation accuracy.

In common semantic segmentation models, cross entropy loss and dice loss are often used as evaluation indicators. The dice value is defined as:

$$Dice = \frac{2 \cdot (x \cap z)}{x \cup z} \tag{8}$$

$$Dice\ Loss = 1 - Dice \tag{9}$$

where x represents manually labelled images and z represents the network segmentation result. When the segmentation result is the same as the manual labelling result, the dice value is 1, or else, the dice loss is 0. Dice values range from 0 to 1.

The dataset used in this study had unbalanced positive and negative samples. Specifically, the black areas in the four corners and outside the cropped ring during data augmentation had a large number of negative samples. Therefore, dice loss cannot accurately reflect the real performance of the network. In order to address the problem of unbalanced samples, the focal loss is used here [34]. Focal loss has some advantages when compared with cross entropy loss:

$$L_{CE} = \begin{cases} -logy' & , y = 1 \\ -log(1 - y') & , y = 0 \end{cases} \tag{10}$$

$$L_F = \begin{cases} -\alpha(1 - y')^{\gamma} logy' & , y = 1 \\ -(1 - \alpha)y'^{\gamma} \log(1 - y') & , y = 0 \end{cases} \tag{11}$$

where y is the real label, y' is the predicted probability value, α and γ are the focusing parameters. In this article, the value of α is 0.25 and the value of γ is 2. For binary classification, $y = 1$ is a positive sample, $y = 0$ is a negative sample, $y' >> 0.5$ is a predicted positive sample, and $y' << 0.5$ is a predicted negative sample. When y' is close to 0.5, the sample is hard to predict. Positive samples can be regarded as the target of detection and negative samples as the back-ground. Difficult samples are those that humans can understand but machines cannot.

IV. Experiments and Results

During the preliminary experiment, we have completed the collection of DHP images at the research area. From October 2021 to May 2022, a total of 300 DHP images were collected and manually annotated with Labelme software [35]. After augmentation, the dataset contained a total of 6000 images for the next model training. In this dataset, the training, validation and testing set are divided by a ratio of 7:2:1. Python 3.8 and MATLAB 2021a are used for modeling and statistical analysis.

A. Assessment of LAINET

Training and evaluation of the LAINET were carried out on the server. The CPU is Intel(R) i5-12600KF 3.70 GHz, the GPU is NVIDIA RTX3060Ti (8 GB memory), the RAM is 16 GB, and the operation system is Ubuntu v20.04. The network model is built in PyTorch. This section detailed evaluates the semantic segmentation effect of CNN and the super-resolution results of GAN, respectively.

1) *Results of CNN Semantic Segmentation*

The hyper parameters used for training are as follows: learning rate is 0.001, batch size is 6, and number of epochs is 100. Adam is used as the optimizer and the loss functions are Dice Loss and Focal Loss. For comparison, we also trained the U-Net, the DeepLab [36], the ENet [37], and the SegNet [38]. The performance of these models during training is shown below in Fig. 11.

Comparing with other four neural network models, the convergence of LAINET is the best (convergence when the number of epochs reached 30), followed by ENet and U-Net.

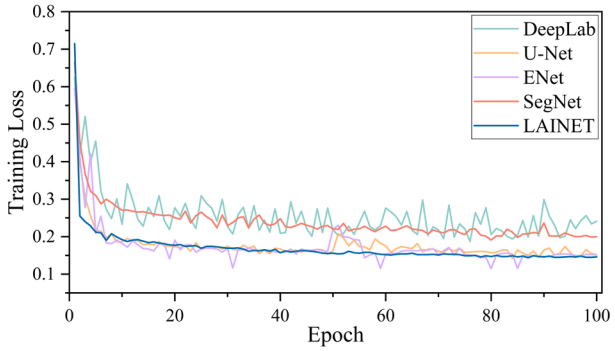

Fig. 11. The training loss of each CNN model.

DeepLab had a sudden increase in the loss value, which is believed to have been caused by a gradient explosion due to overfitting. The condition was relieved after using early stopping, but severe fluctuations were still observed. In terms of accuracy, LAINET also has the highest accuracy (98%), followed by U-Net (92%), while the accuracies of ENet and SegNet were < 90%. The training time of each model was recorded and the F1 score was compared (Table II).

TABLE II
PERFORMANCE COMPARISON OF LAINET AND OTHER CNN MODELS IN TERMS OF F1 SCORE AND TRAINING TIME

CNN	DeepLab	U-Net	ENet	SegNet	LAINET
F1 score	80.62	85.37	82.56	77.48	93.81
Training time	6h50min	10h30min	6h20min	7h30min	8h25min

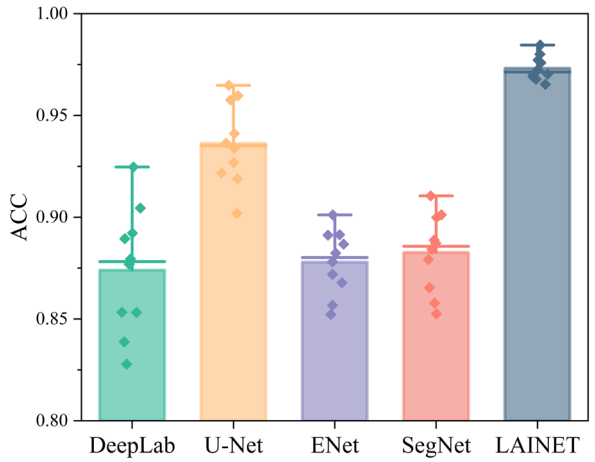

Fig. 12. The mean and standard deviation of model accuracy by repeating tests for ten times.

To further verify the robustness of the neural models, each network model has been trained and validated for 10 times, the mean and variance of the accuracy are calculated in Fig. 12. In the 10 experiments, the average accuracy of LAINET is the highest (97.323%), which is considerably higher than the other models. The variance of LAINET is 0.4927, which is also lower than the other models. Hence, LAINET outperforms the other neural network models in terms of accuracy and robustness.

Fig. 13 shows the segmentation results of different models for plant canopy images. Column (a) is the original image, column (b) is the DeepLab results, column (c) is the U-Net results, column (d) is the ENet results, column (e) is the SegNet results, and column (f) is the LAINET results. It can be seen that the LAINET model proposed in this study has the best performance among the CNN models.

Nonetheless, GPU has also been occupied in the above experiments, so the performance of each model did not indicate the performance of embedded wireless sensor exactly. In our study, all the five trained models were deployed in Raspberry Pi to perform predictions. We recorded the time consumed and the accuracy of estimation results, all the relevant data are shown in Table III. In the dataset of forest canopy images, ENet has the fastest segmentation speed but also the lowest accuracy. LAINET just has the highest accuracy of 97.8%, and the second fastest speed. Thus LAINET is the optimal choice for the wireless sensor in both running speed and detection accuracy.

TABLE III
PERFORMANCE COMPARISON OF LAINET AND OTHER CNN MODELS IN TERMS OF AVERAGE TESTING ACCURACY AND PREDICTING TIME FOR SINGLE IMAGE

CNN Model	DeepLab	U-Net	ENet	SegNet	LAINET
ACC	0.857	0.932	0.791	0.822	0.978
Predicting time	23s	63s	9s	71s	19s

2) *Results of GAN Super Resolution*

In this section, we train and test the lightweight SRGAN, i.e. the original SRGAN while replacing part of the normal convolution with depthwise separable convolution. Some of the relevant training parameters are shown in Table IV.

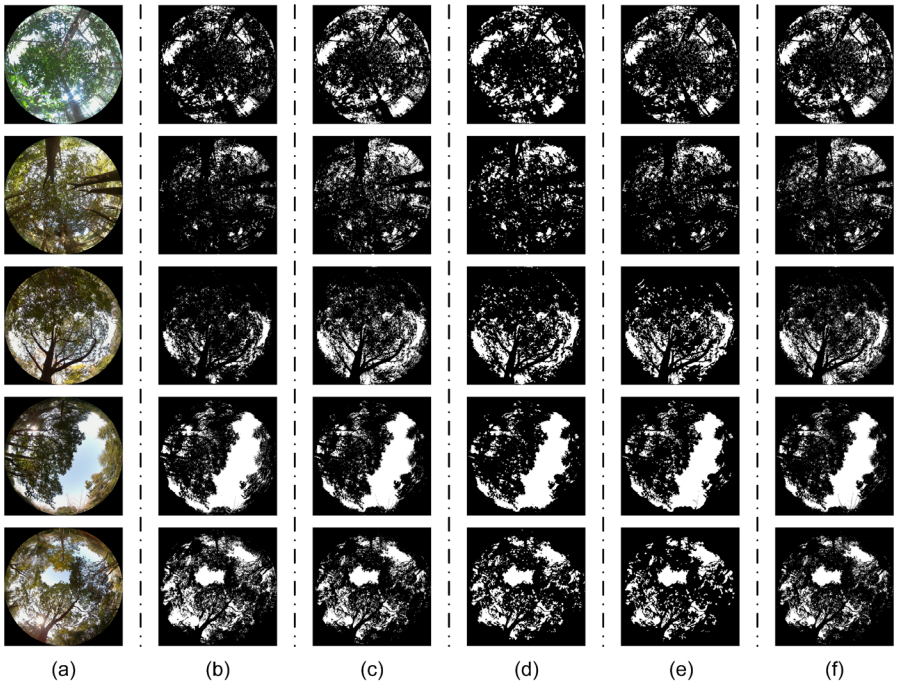

Fig. 13. Practical effects of five segmentation methods.

This article has been accepted for publication in IEEE Sensors Journal. This is the author's version which has not been fully edited and content may change prior to final publication. Citation information: DOI 10.1109/JSEN.2022.3188697

TABLE IV
PERFORMANCE COMPARISON OF SRGAN AND PROPOSED SRGAN IN TERMS OF PSNR, SSIM AND MOS

GAN Kind	PSNR	SSIM	MOS
SRGAN	32.70	0.9268	3.83
Proposed SRGAN	32.51	0.9017	3.87

TABLE V
TIME CONSUMED FOR SUPER-RESOLUTION OF A SINGLE IMAGE USING SRGAN AND PROPOSED SRGAN

GAN	RTX3060Ti	i7-1165G7	Raspberry Pi
SRGAN	3s	15s	27s
Proposed SRGAN	2s	12s	22s

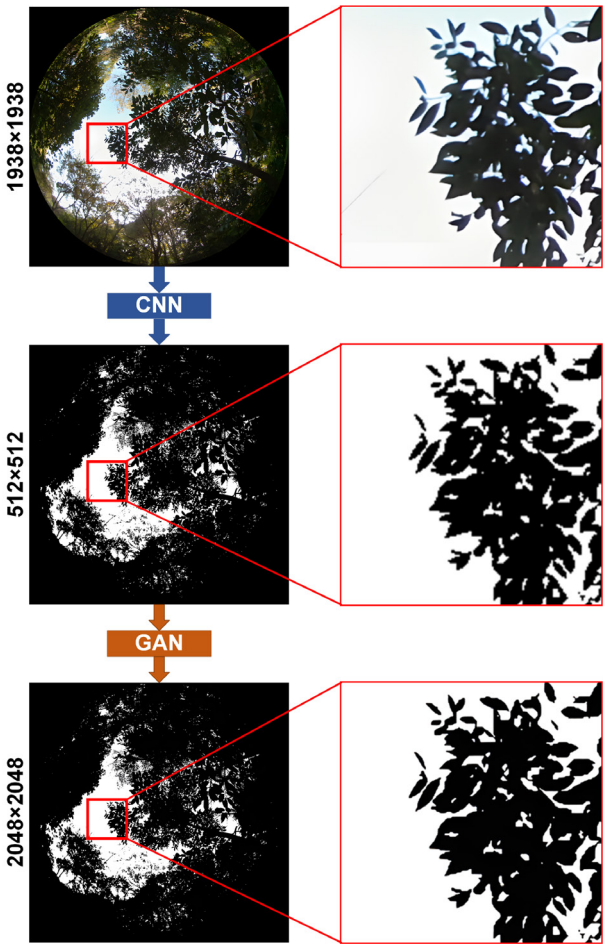

Fig. 14. The detailed effect of proposed SRGAN.

From the training data results, the use of depthwise separable convolution has little effect on the performance of SRGAN, but there is a large difference in the time taken by the network to predict a single image. Table V shows the time consumed to run the network for predicting a single image using RTX3060, laptop CPU i7-1165G7 and Raspberry Pi, and it can be seen that the lightweight SRGAN is more suitable for deployment on low computing power platforms.

Fig. 14 shows the effect of super-resolution on the image using proposed SRGAN. The image pre-processing process has been explained in the previous part, i.e., the size of the image output from CNN is also 512 × 512, and the difference between the original image with it can be clearly seen after enlarging the details, so if it is directly used for the gap fraction, there must bring quite a few errors. Yet after the SRGAN super-resolution proposed in this paper, the image size rises to 2048 × 2048, at which the segmentation effect of the images is much closer to

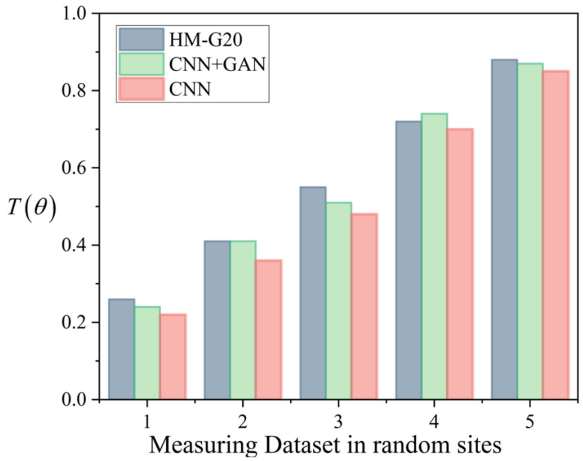

Fig. 15. The gap fraction calculation results of three scenarios.

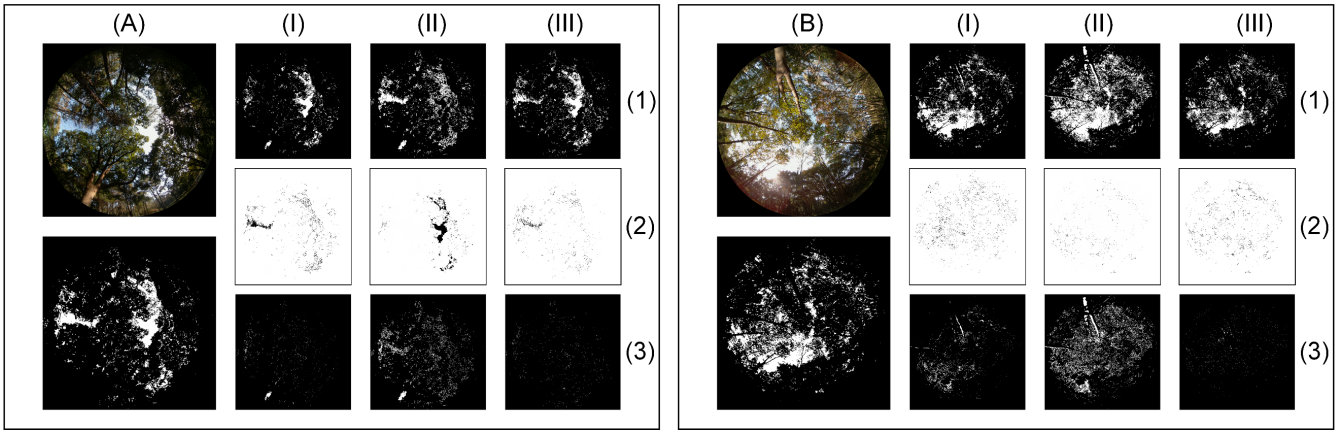

Fig. 16. Comparison of the results of segmenting forest canopy images using LAINET and the traditional method.

the real situation. Fig. 15 just shows the gap fraction results of five datasets measured by HM-G20, LAINET output with CNN and LAINET output with CNN+GAN separately, it could be clearly inferred that the average exaction accuracy of gap fraction has improved by 5.5%.

3) *Comparison with Traditional Methods*

In order to verify the advantages of neural networks in forest canopy image processing over the traditional threshold segmentation method, a comparative experiment has designed and the result is shown in Fig. 16.

Fig. 16(a) and (b) are fisheye images of forest canopies taken under sunny day without direct sunlight and sunny day with direct sunlight, respectively. The color image is the original image taken, the black and white image is the artificially labeled image, the white area is the sky background, and the black area is the vegetation. Columns (I) (II) (III) show the segmentation statuses using the Otsu method, HSV threshold method and LAINET, respectively. Row (1) is the output results, Row (2) is the TN maps, i.e., the sky is misjudged as vegetation, and Row (3) is the FP maps, i.e., vegetation is misjudged as the sky.

Group (a) mainly verifies the effect of blue sky on the threshold segmentation. From the TF figures, we can see that the two traditional segmentation methods cannot effectively separate the sky from the vegetation, and a large number of skies are mistakenly judged as forest; while the segmentation effect of LAINET is relatively satisfactory, and the two main sky backgrounds in the figure have been well handled.

Group (b) mainly verifies the effect of direct sunlight on threshold segmentation, and it can be seen from the FP map that there are many leaves been mistake-segmented as the sky near the sunlight source, and even some tree trunks are affected by direct sunlight causing the skewing of color threshold. Hence the traditional algorithms partially segment the tree trunks as sky, resulting in a large number of FP pixels. LAINET performs significantly better in this situation.

B. Results of LAI Measurement

Gap fraction can be computed based on forest canopy image segmentation and the LAI could be subsequently obtained. Because it is extremely difficult to collect all leaves and calculate the LAI manually, the HM-G20 plant canopy analyzer was used as reference. It should be noted that the HM-G20 has a similar measuring function with LAI-2200C and has been widely used in the agricultural and forestry research in China.

Fig. 17 shows the measurement results of wireless sensor and forest canopy analyzer. A total of 20 scenes were tested. The red dots in the figure represent the measurement results of HM-G20, whereas the blue dots represent the results of DHP sensor in the corresponding inspection positions. After calculation, the maximum error between the proposed sensor and the measuring apparatus in these 20 datasets is 4%, while the average error is 2.95%, which is absolutely within an acceptable range.

To verify that the proposed DHP sensor can be affected by negative external factors such as direct sunlight or not, we carried out a further examination separately on a sunny and a cloudy weather time. Here the HM-G20, the proposed sensor with LAINET, and the proposed sensor using the Otsu method were deployed and measured, respectively. The wireless sensor has been placed in the field for one day of continuous measurement. Fig. 18 shows the results from 8:00 am to 4:00 pm where the upper part is the measurement result on sunny day and the bottom part is the result on cloudy day. It can be seen that on both days, the data measured by the LAINET sensor 1 were stable and consistent with the HM-G20 values, effectively indicating the robustness of proposed mechanism. In contrast, the sensor 2 using Otsu method showed large fluctuations in measured values during clear weather, which is closely related with the azimuth of direct solar radiation. Nevertheless, all its measured result was significantly smaller comparing with the previous two, which is also related to the inherent inaccuracy of the traditional threshold segmentation method.

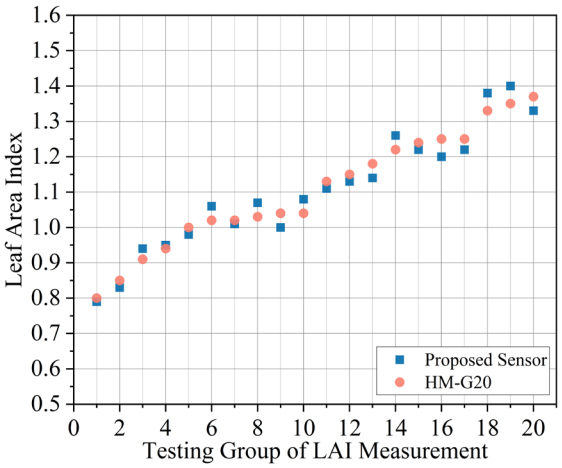

Fig. 17. Comparison of leaf area index measured by proposed wireless sensor and handheld measuring instrument.

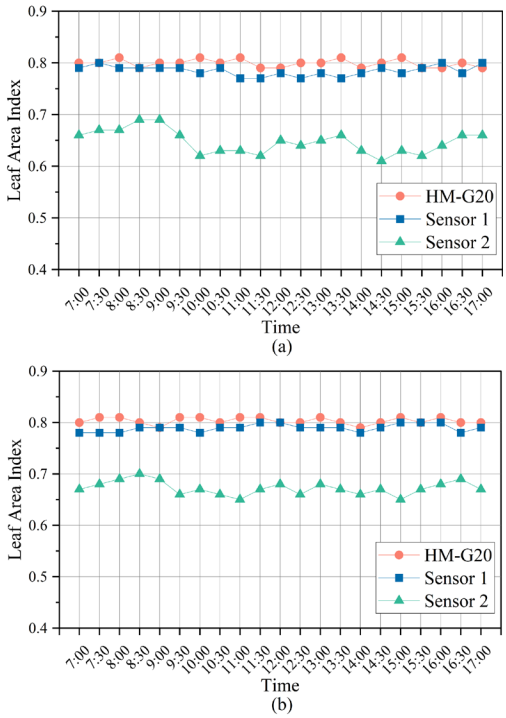

Fig. 18. Monitoring data of leaf area index from 7 am to 5 pm using the proposed sensor.

C. Power Consumption

The power consumption of proposed sensor is a key factor for its long term deployment in the field. In this section, we compare and evaluate its energy consumption characteristic by a dedicated experiment: 5 LAI detection algorithms (including traditional and deep learning methods) are implemented on the designed sensors individually and they have been placed and tested in the field for 10 consecutive days, respectively. The sensors would measure and transmit data twice a day (10 am and 4 pm), and their energy variations have been stored. The corresponding results are shown in Fig. 19.

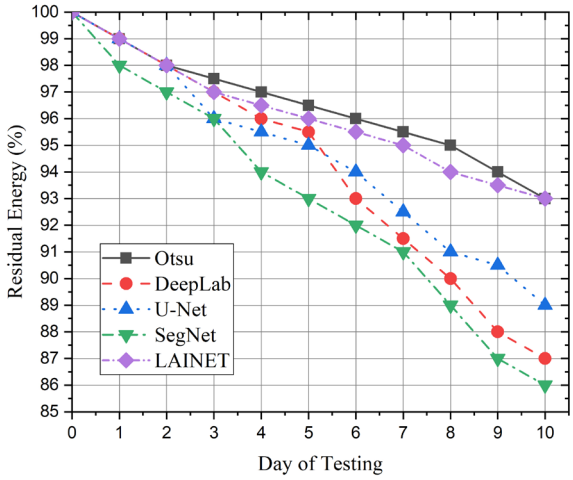

Fig. 19. Energy consumption of wireless DHP nodes under different operating mechanisms with initial batteries 5200 mAh.

As can be seen, the power consumption of LAINET mechanism proposed in this paper is slightly higher than that of traditional Otsu method, but obviously lower than that of other deep learning algorithms. According to the practical detection requirement, normally one reports per day should be carried out. So it can be estimated that the working life of the proposed sensor node with LAINET could last for at least 8 months without human intervention, about 2 times of other artificial intelligence methods, which meets the measurement criteria of conventional forestry resource inventory.

D. Discussion

Section *A* discussed the performance of LAINET proposed in this work. Compared with other CNN models, LAINET has the characteristics of good convergence and high prediction accuracy. The segmentation result of LAINET was obviously better than other CNN models. Meanwhile, thanks to the introduction of SRGAN super-resolution mechanism, the image segmentation precision in this paper has been significantly improved. As far as we know, this is the first time that the super-resolution algorithm has been introduced into this field. Compared with the traditional threshold segmentation algorithms HSV and Otsu, the proposed algorithm has better segmentation effect, especially in the case of direct sunlight or unsatisfactory illumination conditions.

In the comparison experiment with the hand-held measuring instrument HM-G20, the analysis results in Section *B* reflected that the sensor designed here is highly correlated with the measurement results of the hand-held measuring instrument. Due to its easy installation feature, the sensor could fully meet the practical measurement needs.

The power consumption has been studied in section *C*. It can be figured from the evaluation outcomes that the sensor designed has the characteristic of ultra-low power consumption. It is deduced that its working life can reach about more than half a year, which meets the installation requirements of forestry Internet of Things.

To sum up, the wireless DHP sensor presented in this paper solves some problems faced by remote LAI measurement nowadays and can replace the manual detection scheme to achieve a large-scale deployment and automatic data collection.

V. Conclusion

In this present research, we built a wireless DHP sensor for LAI measurement which is composed of a Raspberry Pi and a novel lightweight neural network, LAINET, which allowed for the remote automatic measuring of forestry LAI. The semantic segmentation performance of proposed LAINET has been comprehensively verified by comparing with other neural models and traditional segmentation methods. The accuracy of wireless DHP sensor was examined by calibrating the measurement results with a commercial plant canopy analyzer. Finding proves that the designed sensor node can work efficiently and effectively. Compared with the image semantic segmentation method using CNN alone, our method combining CNN and GAN together could offset the pixel information loss caused by CNN training, restore image detail information better, therefore, more suitable for the LAI field monitoring. In general, the sensor nodes designed in this paper can actually replace the traditional artificial LAI measurement methods, which strongly promotes the development of forestry Internet of Things technology.

In future work, we will aim to introduce a super lightweight neural network while ensuring the segmentation accuracy to further reduce the computing power requirements for the embedded device. Moreover, multiple wireless LAI sensor nodes and the server can be connected to form an artificial internet of things system to realize adaptive federated learning, thereby greatly improving the accuracy and robustness of the forestry monitoring network.

References

[1] M. Henry et al., "An overview of existing and promising technologies for national forest monitoring," *Annals of Forest Science*, vol. 72, no. 6, pp. 779–788, Sep. 2015.

[2] PJ. Shi, KX. Yu, U. Niinemets, and J. Gielis, "Can Leaf Shape be represented by the Ratio of Leaf Width to Length? Evidence from Nine Species of Magnolia and Michelia (Magnoliaceae)," *Forests (Basel)*, vol. 12, no. 1, Jan. 2021, Art. No. 41.

[3] CDM. Martins, D. Schmitt, PG. Duchini, T. Miqueloto, and AF. Sbrissia, "Defoliation intensity and leaf area index recovery in defoliated swards: implications for forage accumulation," *Scientia Agricola*, vol. 78, no. 2, 2021, Art. No. e20190095.

[4] ZL. Liu, GZ. Jin, JM. Chen, YJ. Qi. "Evaluating optical measurements of leaf area index against litter collection in a mixed broadleaved-Korean pine forest in China," *Trees*, vol. 29, pp. 59–73, Feb.2015.

[5] H. Lee, J. Park, S. Cho, M. Lee, H.S. Kim. "Impact of leaf area index from various sources on estimating gross primary production in temperate forests using the JULES land surface model," *Agricultural and Forest Meteorology*, vol. 276-277, Jun. 2019, Art. No. 107614.

[6] Hongliang. Fang, "Canopy clumping index (CI): A review of methods, characteristics, and applications," *Agricultural and Forest Meteorology*,

vol. 303, Jun. 2021, Art. No. 108374.
[7] HL. Fang, YC. Ye, WW. Liu, SS. Wei, and L. Ma, "Continuous estimation of canopy leaf area index (LAI) and clumping index over broadleaf crop fields: An investigation of the PASTIS-57 instrument and smartphone applications," *Agricultural and Forest Meteorology*, vol. 253-25, pp. 48–61, May. 2018.
[8] Y. Ryu, J. Verfaillie, C. Macfarlane, H. Kobayashi, O. Sonnentag, R. Vargas, S, Ma, and DD. Baldocchi, "Continuous observation of tree leaf area index at ecosystem scale using upward-pointing digital cameras," *Remote Sensing of Environment*, vol. 126, pp. 116–125, Nov. 2012.
[9] LA. Brown, C. Meier, H. Morris, J. Pastor-Guzman, G. Bai, C. Lerebourg, N. Gobron, C. Lanconelli, M. Clerici, and J. Dash, "Evaluation of global leaf area index and fraction of absorbed photosynthetically active radiation products over North America using Copernicus Ground Based Observations for Validation data," *Remote Sensing of Environment*, vol. 247, Sep. 2020, Art. No. 111935.
[10] J. Mendes, TM. Pinho, FN. Dos Santos, JJ. Sousa, E. Peres, J. Boaventure-Cunha, M. Cunha, and R. Morais, "Smartphone Applications Targeting Precision Agriculture Practices-A Systematic Review," *Agronomy (Basel)*, vol. 10, no. 6, Jun. 2020, Art. No. 855.
[11] YH. Qu, ZX. Wang, JL. Shang, JG. Liu, and J. Zou, "Estimation of leaf area index using inclined smartphone camera," *Computers and Electronics in Agriculture*, vol. 191, Dec. 2021, Art. No. 106514.
[12] LA. Brown, DH. Sutherland, and J. Dash, "Low-cost unmanned aerial vehicle-based digital hemispherical photography for estimating leaf area index: a feasibility assessment," *International Journal of Remote Sensing*, vol. 41, no. 23, pp. 9064–9074, Sep. 2020.
[13] B. Su, Z. Qin and Q. Ni, "Energy Efficient Uplink Transmissions in LoRa Networks," *IEEE Transactions on Communications*, vol. 68, no. 8, pp. 4960-4972, Aug 2020.
[14] XH. Li, Q. Liu, RJ. Yang, HJ. Zhang, JL. Zhang, and E. Cai, "The design and implementation of the leaf area index sensor," *Sensors (Basel)*, vol. 15, no. 3, pp. 6250–6269, Mar. 2015.
[15] J. Bauer, T. Jarmer, S. Schittenhelm, B. Siegmann, and N. Aschenbruck, "Processing and filtering of leaf area index time series assessed by in-situ wireless sensor networks," *Computers and Electronics in Agriculture*, vol. 165, Oct. 2019, Art. No. 104867.
[16] J. Kim, Y. Ryu, C. Jiang, and Y. Hwang, "Continuous observation of vegetation canopy dynamics using an integrated low-cost, near-surface remote sensing system," *Agricultural and forest meteorology,* vol. 264, pp. 164–177, Jan. 2019.
[17] YX. Li, HJ. Liu, JC. Ma, and LX. Zhang, "Estimation of leaf area index for winter wheat at early stages based on convolutional neural networks," *Computers and Electronics in Agriculture*, vol. 190, Sep. 2021, Art. No. 106480.
[18] WQ. Shu, L. Wang, BL. Liu, and J. Liu, "LAI Estimation of Cucumber Crop Based on Improved Fully Convolutional Network," *arXiv preprint arXiv: 2104.07955*, 2021.
[19] Cunshi. Ma et al., "Deep Learning for Vegetation Image Segmentation in LAI Measurement," in *IEEE International Geoscience and Remote Sensing Symposium (IGARSS)*, Waikoloa, HI, USA, Sep. 2020, pp. 940–943.
[20] RF. Deng, YB. Lin, WJ. Tang, FS. Gu, and A. Ball, "Object-Based Thermal Image Segmentation for Fault Diagnosis of Reciprocating Compressors," *Sensors (Basel)*, vol. 20, no. 12, Jun. 2020, Art. No. 3436.
[21] S. Rapaka, PR. Kumar, "Efficient approach for non-ideal iris segmentation using improved particle swarm optimisation-based multilevel thresholding and geodesic active contours," *IET Image Processing*, vol. 12, no. 10, pp. 1721–1729, Oct. 2018.
[22] R. Mahmud, AN. Toosi, "Con-Pi: A Distributed Container-Based Edge and Fog Computing Framework," *IEEE Internet of Things Journal*, vol. 9, no. 6, pp. 4125–4138, Mar. 2022.
[23] TY. Wu, S. Tang, R. Zhang, J. Cao, and YD. Zhang, "CGNet: A Light-Weight Context Guided Network for Semantic Segmentation," *IEEE Transactions on Image Processing*, vol. 30, pp. 1169–1179, Jan. 2021.
[24] Christian Ledig etal., "Photo-Realistic Single Image Super-Resolution Using a Generative Adversarial Network," in *Proc. IEEE Conference on Computer Vision and Pattern Recognition (CVPR)*, Honolulu, HI, USA, Jul. 2017, pp. 105–114.
[25] F. Scholkmann, S. Kleiser, AJ. Metz, R. Zimmermann, JM. Pavia, U. Wolf, and M. Wolf, "A review on continuous wave functional near-infrared spectroscopy and imaging instrumentation and methodology," *Neuroimage*, vol. 85, no. S1, pp. 6–27, Jan. 2014.
[26] J. Pisek, Y. Ryu, K. Alikas, "Estimating leaf inclination and G-function from leveled digital camera photography in broadleaf canopies," *Trees-Structure and Function*, vol. 25, no. 5, pp. 919–924, Oct. 2011.
[27] HM-G20. Shandong Hengmei Electronic Technology Co., Ltd, China. Accessed: Mar. 30, 2022. [Online]. Available: https://www.hmdzkj.com/product/170.html
[28] P. Sukic, and G. Gtumberger, "Intra-Minute Cloud Passing Forecasting Based on a Low Cost IoT Sensor-A Solution for Smoothing the Output Power of PV Power Plants," *Sensors (Basel)*, vol. 17, no. 5, May. 2017, Art. No. 1116.
[29] O. Ronneberger, P. Fischer and T. Brox, "U-Net: Convolutional networks for biomedical image segmentation," in *Proc. Int. Conf. Med. Image Comput. Comput.-Assisted Intervention*, Munich, Germany, Oct. 2015, pp. 234–241.
[30] P. Korfiatis, TL. Kline, DH. Lachance, IF. Parney, JC. Buckner, and BJ. Erickson, "Residual Deep Convolutional Neural Network Predicts MGMT Methylation Status," *Journal of Digital Imaging*, vol. 30, no. 5, pp. 622–628, Oct. 2017.
[31] A. Howard, M. Zhu, B. Chen, D. Kalenichenko, W. Wang, T. Weyand, et al., "Mobilenets: Efficient convolutional neural networks for mobile vision applications," *arXiv preprint arXiv: 1704.04861*, Apr. 2017.
[32] Ross Girshick, "Fast R-CNN," in *Proc. IEEE International Conference on Computer Vision (ICCV)*, Santiago, Chile, Dec. 2015, pp. 1440–1448.
[33] K. Prajapati et al., "Direct Unsupervised Super-Resolution Using Generative Adversarial Network (DUS-GAN) for Real-World Data," *IEEE Transactions on Image Processing*, vol. 30, pp. 8251–8264, Sep. 2021.
[34] T.Y. Lin, P. Goyal, R. Girshick, KM. He and P. Dollár, "Focal Loss for Dense Object Detection," *IEEE Transactions on Pattern Analysis and Machine Intelligence*, vol. 42, no. 2, pp. 318–327, Feb. 2020.
[35] LabelMe. MIT, Computer Science and Artificial Intelligence Laboratory, USA. Accessed: Mar. 30, 2022. [Online]. Available: http://labelme2.csail.mit.edu/Release3.0/index.php?message=1
[36] L.C. Chen, G. Papandreou, I. Kokkinos, K. Murphy and A. L. Yuille, "DeepLab: Semantic Image Segmentation with Deep Convolutional Nets, Atrous Convolution, and Fully Connected CRFs," *IEEE Transactions on Pattern Analysis and Machine Intelligence*, vol. 40, no. 4, pp. 834–848, Apr. 2018.
[37] A. Paszke, A. Chaurasia, S. Kim, and E. Culurciello, "ENet: A Deep Neural Network Architecture for Real-Time Semantic Segmentation," *arXiv preprint arXiv: 1606.02147*, Jun. 2016.
[38] V. Badrinarayanan, A. Kendall, and R. Cipolla, "SegNet: A deep convolutional encoder-decoder architecture for image segmentation," *IEEE Transactions on Pattern Analysis and Machine Intelligence*, vol. 39, no. 12, pp. 2481–2495, Oct. 2016.

Hancong Wang (Student Member, IEEE) is currently a student at College of Information Science and Technology, Nanjing Forestry University, Nanjing, China. He became a Student Member of IEEE in 2021. His research interests include IoT-based forestry technologies and AI computing systems.

Yin Wu was born in China, in 1982. He received the Ph.D. degree from the Department of Test Engineering, Nanjing University of Aeronautics and Astronautics, Nanjing, China, in 2013. He is currently an Associate Professor with the College of Information Science and Technology, Nanjing Forestry University, Nanjing. His main research interests are energy harvesting wireless sensor networks, forestry measurement systems, and wood structural health monitoring.

This article has been accepted for publication in IEEE Sensors Journal. This is the author's version which has not been fully edited and content may change prior to final publication. Citation information: DOI 10.1109/JSEN.2022.3188697

Qiang Ni (Senior Member, IEEE) received the B.Sc., M.Sc., and Ph.D. degrees in engineering from the Huazhong University of Science and Technology, China. He led the Intelligent Wireless Communication Networking Group with Brunel University London, U.K. He is currently a Professor and the Head of the Communication Systems Group, InfoLab21, School of Computing and Communications, Lancaster University, Lancaster, U.K. His main research interests lie in the areas of wireless communications and networking, including green communications, cognitive radio systems, 5G, Internet-of-Things, and vehicular networks. He was an IEEE 802.11 Wireless Standard Working Group Voting Member and a Contributor to the IEEE Wireless Standards.

Wenbo Liu received the Ph.D. degree from the Department of Test Engineering, Nanjing University of Aeronautics and Astronautics, Nanjing, China. She is currently a Professor with the College of Automation, Nanjing University of Aeronautics and Astronautics. Her main research interests lie in the areas of deep learning, digital signal processing, and nonlinear system control.